Preparation and Characterization of Carbon Nanospheres as Anode Materials in Lithium-Ion Secondary Batteries

ARTICLE *in* INDUSTRIAL & ENGINEERING CHEMISTRY RESEARCH · FEBRUARY 2008

Impact Factor: 2.59 · DOI: 10.1021/ie071337d

Preparation and Characterization of Carbon Nanospheres as Anode Materials in Lithium-Ion Secondary Batteries

Yong Wang,[†,‡] Fabing Su,*[,†,§] Colin D. Wood,[§] Jim Yang Lee,[†] and Xiu Song Zhao*[,†]

Department of Chemical and Biomolecular Engineering, National University of Singapore, 4 Engineering Drive 4, Singapore 117576; Department of Chemical Engineering, School of Environmental and Chemical Engineering, Shanghai University, Chengzhong Road No. 20, Jiading, Shanghai, People's Republic of China 201800; and Department of Chemistry, University of Liverpool, Crown Street, Liverpool L69 3BX, United Kingdom

Carbon nanospheres (CNSs) with a diameter of less than 100 nm, containing nitrogen-functional groups, and turbostratic structure were prepared by carbonizing polypyrrole nanospheres (PNSs), which were synthesized by polymerization of pyrrole under ultrasonic conditions in the presence of dual surfactants and catalyst. The materials were characterized by X-ray diffraction, thermogravimetric analysis, field-emission transmission electron microscope, field-emission scanning electron microscope, Raman spectroscope, nitrogen adsorption, and X-ray photoelectron spectroscope. In addition, the electrochemical properties of the CNSs as anode materials in lithium-ion batteries were evaluated. It was found that the use of ultrasonication is a simple and reproducible method for the synthesis of monodisperse PNSs. The CNSs displayed a higher specific capacity than the carbon spheres derived from sucrose and a higher rate capability than commercial mesophase carbon microbeads.

1. Introduction

Spherical carbon particles have received growing research attention because of their applications as catalyst supports, column packing materials, lubricating materials, and reinforced rubber additives. In general, there are three approaches to the preparation of carbon spheres: First, they can be directly synthesized using methods such as chemical vapor deposition,[1] pyrolysis,[2,3] and hydrothermal treatment.[4] Second, templating techniques using hard templates can be employed.[5,6] The third method is to first synthesize polymer spheres, followed by a thermal treatment in an inert atmosphere to obtain carbon spheres.[7−15] However, despite the fact that there are a large number of reports on the synthesis of spherical carbon particles, the number of publications on carbon nanospheres (CNSs) (<100 nm) is limited.[14,15]

Of the approaches listed above, the third is more favorable since the size of carbon spheres could potentially be controlled by tuning the diameter of the polymer spheres. Thus, a facile method for the synthesis of polymer nanospheres, which can be subsequently converted to carbon nanospheres with a controllable particle size, is highly desirable.

Polypyrrole (Ppy) that has been prepared by the polymerization of pyrrole in the presence of an oxidative catalyst[16] is a technologically important, environmentally stable, and biocompatible conducting polymer. Various nanostructures and morphologies of Ppy have been produced by Jang's and Manohar's groups, such as crystalline lamellar structures,[11] nanoparticles,[15] core−shell nanoparticles,[12] nanofibers,[17] and nanotubes.[18,19] These nanostructured Ppy can subsequently be carbonized to produce carbon materials.

CNSs can be used in many emerging applications such as anode materials for lithium-ion batteries,[20,21] novel catalyst supports,[22] cell delivery systems,[23] photoluminescence,[24] and multiphoton bioimaging.[25] Recently, lithium-ion batteries have attracted widespread attention because of their commercial applications ranging from small portable electronic devices to large modules for hybrid-electric vehicles. Requirements such as high-rate performance, long life, high reversible capacity, and safety are essential for the widespread use of lithium-ion batteries. The electrochemical performance of lithium-ion batteries could potentially be enhanced by the improvement of lithium-ion diffusion in anode carbon materials with nanostructures[26−30] or graphitized carbon nanoparticle sizes.[20]

In this work, we report the preparation of turbostratic CNSs with a diameter of <100 nm by carbonizing Ppy nanospheres (PNSs), which were synthesized by the ultrasonication polymerization method instead of using a template strategy,[5,6,11] hydrothermal treatment,[7,8] microwave treatment,[10] microemulsion polymerization,[12] and suspension polymerization.[13,15] This is because the ultrasonication technique offers a fast polymerization rate and reinforced particle dispersion. The electrochemical properties of the CNSs as an anode material in lithium-ion batteries have been investigated.

2. Experimental Section

2.1. Preparation of Materials. In a typical synthesis, 1 g of decyl alcohol (1-decanol, 99%, Aldrich) was added to 30 mL of deionized water with stirring at 1 °C in a refrigerated circulating water bath for 10 min. Then, 1.5 g of dodecyltrimethylammonium bromide (DTAB, 99%, Aldrich) was added under stirring at 1 °C for 20 min. The mixture was then transferred into a plastic tube, and a specific amount of pyrrole (98%, Aldrich) was then added dropwise into the tube under ultrasonication (Elma Transsonic T460/H of capacity 2.75 L and frequency of 35 kHz). After 2 min, 2 g of $FeCl_3$ (99%, Aldrich) was added. After further ultrasonication for 30 min, the resultant products, PNSs, were separated by filtration,

* To whom correspondence should be addressed. Tel.: +44-07794848310 (F.S.), +65-65164727 (X.S.Z.). Fax: +44-1517943588 (F.S.), +65-67791936 (X.S.Z.). E-mail: fabing.su@liverpool.ac.uk (F.S.), chezxs@nus.edu.sg (X.S.Z.).

[†] National University of Singapore.

[‡] Shanghai University.

[§] University of Liverpool.

washed with ethanol and water, and dried at 60 °C overnight in a vacuum oven. Different amounts of pyrrole (0.8, 0.5, and 0.2 g) were used, and the PNS samples thus obtained are denoted as PNS-1, PNS-2, and PNS-3, respectively. The yield of PNSs relative to the pyrrole amount added was in the range of 80−90 wt %. The PNSs were carbonized in a quartz tube at 900 °C for 2 h under a nitrogen atmosphere to obtain CNSs, designated as CNS-1, CNS-2, and CNS-3, respectively.

2.2. Material Characterization. Physical adsorption of nitrogen was conducted at 77 K on an automatic volumetric sorption analyzer (Quantachrome, NOVA1200). Prior to the measurement, the samples were degassed at 200 °C for 5 h under vacuum. The specific surface areas were determined according to the Brunauer−Emmett−Teller (BET) method in the relative pressure range of 0.05−0.20. The X-ray diffraction (XRD) patterns were collected on an XRD-6000 (Shimadzu, Japan) with Cu Kα radiation of wavelength $\lambda = 0.15418$ nm. Thermogravimetric analysis (TGA) was conducted on a thermogravimetric analyzer TGA 2050 (Thermal Analysis Instruments, U.S.A.) in either air or nitrogen with a flow rate of 100 mL/min and a ramp of 10 °C/min. The microscopic features of the samples were observed with a field-emission scanning electron microscope (SEM) (JSM-6700F, JEOL Japan) operated at 10 kV and field-emission transmission electron microscope (TEM) (JEM 2010F, JEOL, Japan) operated at 200 kV. Elemental analysis was estimated using an energy dispersive X-ray (EDX) spectroscope. Raman spectra were recorded on a Jobin-Yavon T6400 micro-Raman system at room temperature with an argon-ion laser at an excitation wavelength of 514.5 nm. The surface chemical composition of the samples was determined by X-ray photoelectron spectroscopy (XPS) (Kratos Analytical, AXIS HSI 165 spectrometer) using a monochromatized Al Kα X-ray source (1486.71 eV photons). The operating pressure in the analysis chamber was $<8 \times 10^{-9}$ Torr. Wide-scan spectra in the binding energy range of 1100−0 eV were recorded in a 1 eV step size with a pass energy of 80 eV. The N_{1s} XPS signals were recorded in a 0.05 eV step size with a pass energy of 40 eV. The binding energy (BE) of the XPS spectra was referenced to the C_{1s} electron bond energy of 284.6 eV.

2.3. Measurement of Electrochemical Properties. The performances of the CNSs as anode materials in lithium-ion batteries were measured by two-electrode cells and compared with commercial mesophase carbon microbeads (MCMBs 25−28, Osaka Gas Chemicals). The working electrode consisted of 80 wt % of the active material, 10 wt % of conductivity agent (carbon black, Super-P), and 10 wt % of binder (poly(vinylidene difluoride), PVDF, Aldrich). Lithium foil was used as the counter and reference electrodes. The electrolyte was 1 M $LiPF_6$ in a 50:50 w/w mixture of ethylene carbonate (EC) and diethyl carbonate (DEC). More details on the electrode preparation and cell assembly can be found elsewhere.[31] The cells were charged and discharged galvanostatically at different currents. In all tests, the electrodes had the same thickness and were similarly loaded. The first cycle charging was kept constant at 60 mA/g (current rate = $C/7$, $1C = 420$ mA/g), and the voltage limits were fixed in the range of 2 V−5 mV.

3. Results and Discussion

3.1. SEM Observation. Figure 1 shows the SEM images of polypyrrole (Ppy) particles prepared under different conditions. In a system consisting of water/1-decanol/DTAB/pyrrole = 30 mL/1.0 g/1.5 g/x g, when $x = 0.8$, sample PNS-1 with a monodisperse particle size of ∼100 nm in diameter was obtained. The particle size of the PNSs is closely related to the feeding amount of pyrrole monomers. By decreasing the amount of pyrrole monomer added to the system (0.5 g), this produces sample PNS-2 with a particle size of ∼70 nm in diameter (Figure 1c), whereas when 0.2 g of pyrrole was added, this gave sample PNS-3 with a particle size of ∼50 nm in diameter (see Figure 1d). The cationic surfactant (DTAB) in the aqueous solution generates micelles at the concentration over critical micelle concentration (CMC) because the strength of hydrophobic interactions of hydrocarbon spacers exceeds that of electrostatic repulsions of ionic head groups. The flexibility of the long spacers in DTAB provides free volume inside the micelles employed as nanoreactors for pyrrole polymerization. As the liquid pyrrole was added dropwise into the solution containing the surfactant, the large droplet of liquid pyrrole was initially broken into numerous small ones under extremely powerful ultrasonic vibration that could result in the formation, growth, and collapse of gas/vapor-filled bubbles in a liquid phase, so-called cavitation phenomenon. The cavitation could affect the formation of radicals, mixing of reactants, mass diffusion, and dispersion of particles.[32,33] Since pyrrole monomers have poor solubility in water, these small pyrrole droplets are likely to be introduced into the hydrophobic inner space of DTAB micelles.[11] As the ultrasonication time was extended, these small droplets were split to smaller and stable liquid particles under these experimental conditions. After adding iron catalyst, the Fe^{3+} will diffuse into the micelles to initiate the polymerization of pyrrole monomer, eventually forming PNS particles. At a given DTAB concentration over CMC (7.0×10^{-2} M), the number of surfactant molecules (39[44]) that form micelles is constant and, thus, the number of micelles in a fixed system is constant. Increasing the feed ratio of pyrrole could lead to an increase in the amount of pyrrole in one nanoreactor, resulting in the enlargement of micelle size to some degree.[34] Therefore, the size of PNSs could be tuned to some extent by controlling the feeding monomer amount.

Parts e and f of Figure 1 show the morphology of the Ppy samples prepared in the absence of DTAB and 1-decanol, respectively. Without surfactant, the Ppy particles are nonspherical in shape, indicating the significant role of synergistic interaction between DTAB and 1-decanol in determining particle morphology. Here, 1-decanol was used as a cosurfactant to avoid the diffusion of pyrrole monomers through the aqueous phase in the oil/water micelle system. It has been known that polydisperse polymer nanoparticles are generally formed in a traditional polymerization emulsion system where the aggregation of small droplets to large ones could decrease the chemical potential gradient and lead to diffusional degradation of monomers in micelle droplets. Adding 1-decanol could enhance the size uniformity and stability of micelles.

Additionally, under ultrasonication, the polymerization catalyst ($FeCl_3$) dissolved rapidly and the temperature of liquid was gradually increased because of the acoustic energy transferred. In our experiment, the temperature in the ultrasonic water bath was increased from 1 to 35 °C after 30 min. This increase may have accelerated the polymerization process.

Figure 2 shows the SEM images of carbon sphere samples. It can be seen that the particle sizes of CNS-1 (Figure 2 parts a and b), CNS-2 (Figure 2c), and CNS-3 (Figure 2d) are about 80−90, 60−70, and 40−50 nm, respectively, which are relatively smaller than those of their counterpart PNSs shown in Figure 1. This is due to the shrinkage (ca. 10% in diameter) of PNSs during the thermal treatment process, which led to the formation of denser CNSs accompanied with denitrogenation, dehydrogenation, and aromatization. The rough

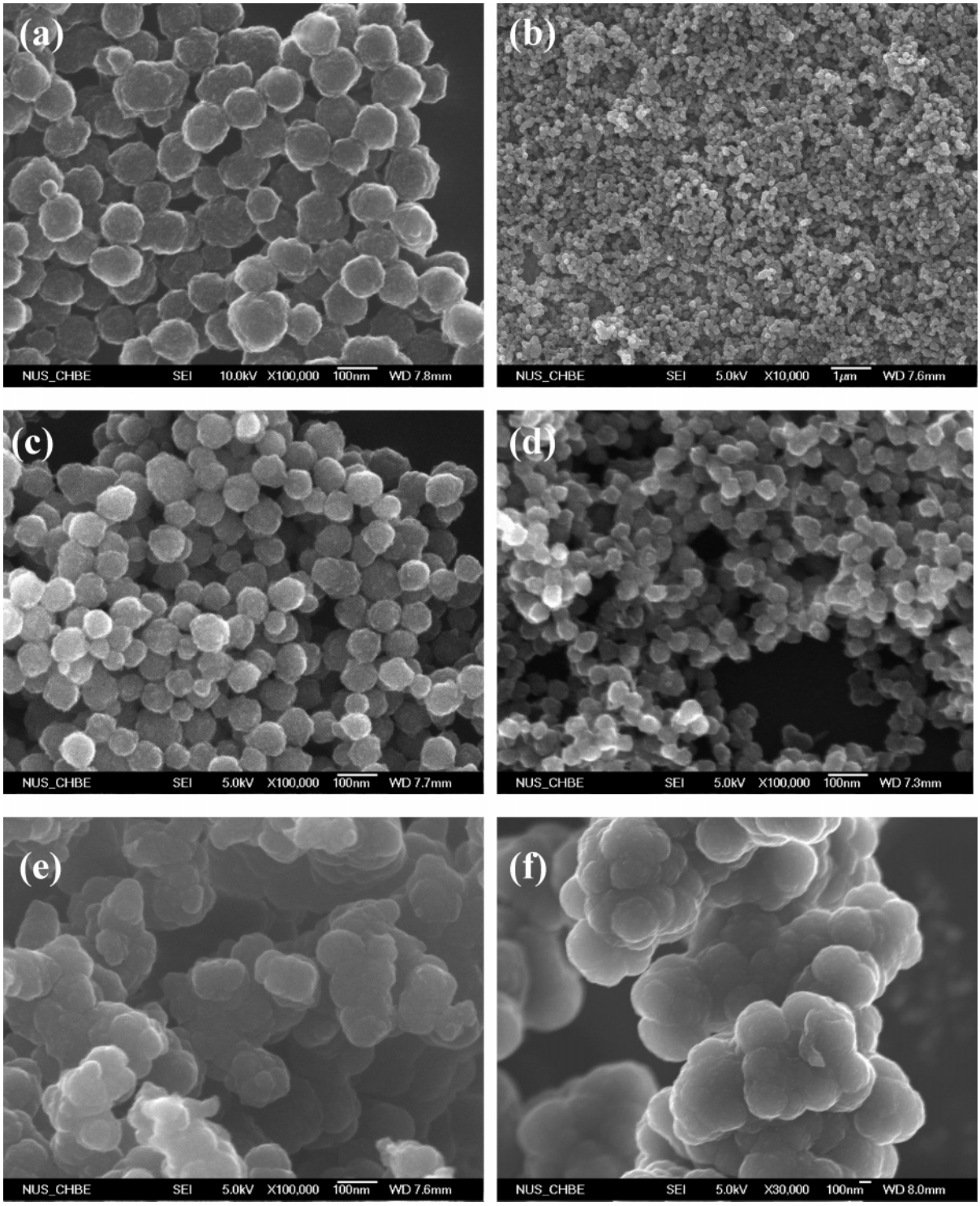

Figure 1. SEM images of polypyrrole particles: (a, b) PNS-1; (c) PNS-2; (d) PNS-3; (e) Ppy particles synthesized without DTAB; and (f) Ppy particles synthesized without 1-decanol.

surface morphology of CNSs shown in Figure 3b indicates that shrinkage occurred heterogeneously during the carbonization process. Therefore, tuning the feed amount of pyrrole monomer may allow one to control the diameter of PNSs and, thus, CNSs.

3.2. TEM Observation. Figure 3a shows the TEM images of sample CNS-2 at different magnifications. The particle size is in the range of 60−70 nm in diameter, consistent with the SEM observation in Figure 2c. The TEM image shown in the inset of Figure 3a clearly reveals the presence of stacked graphene layers roughly parallel to the surface of CNS, indicating a turbostratic structure. The carbonization temperature (900 °C) is not high enough to improve the local order of these formed layers. These layers in general also possess some dangling bonds at the graphene edges, offering opportunities for interaction with other molecules for surface modification.[2] Figure 3b shows the EDX spectrum of sample CNS-2, showing the presence of C (84 wt %), N (7 wt %), O (6 wt %). and Fe (3 wt %).

3.3. XRD and Raman Analysis. Figure 4a shows the XRD patterns of samples PNS-2 and CNS-2. Two peaks at around 25 and 43° 2θ can be seen for CNS-2. These two broad peaks

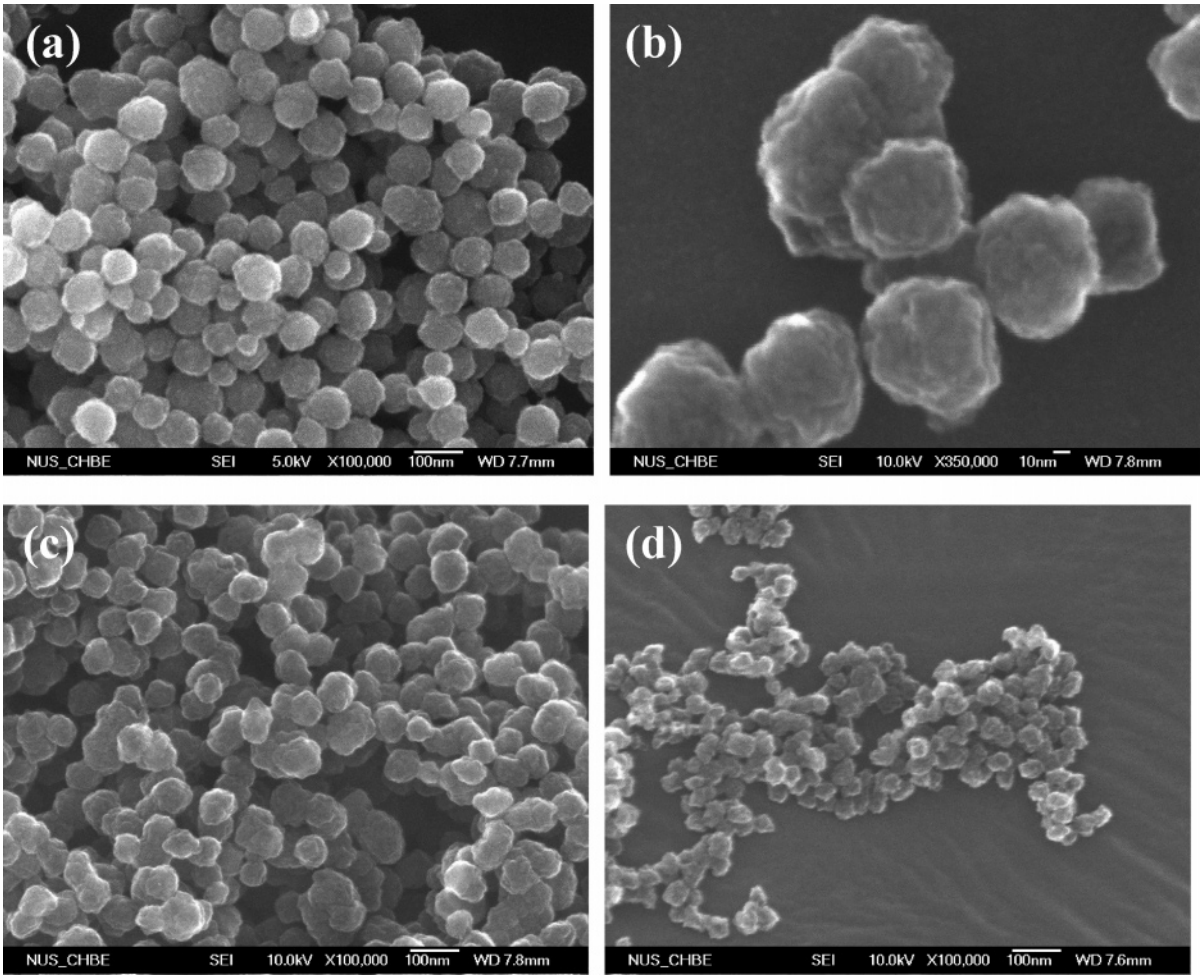

Figure 2. SEM images: (a,b) CNS-1; (c) CNS-2; and (d) CNS-3.

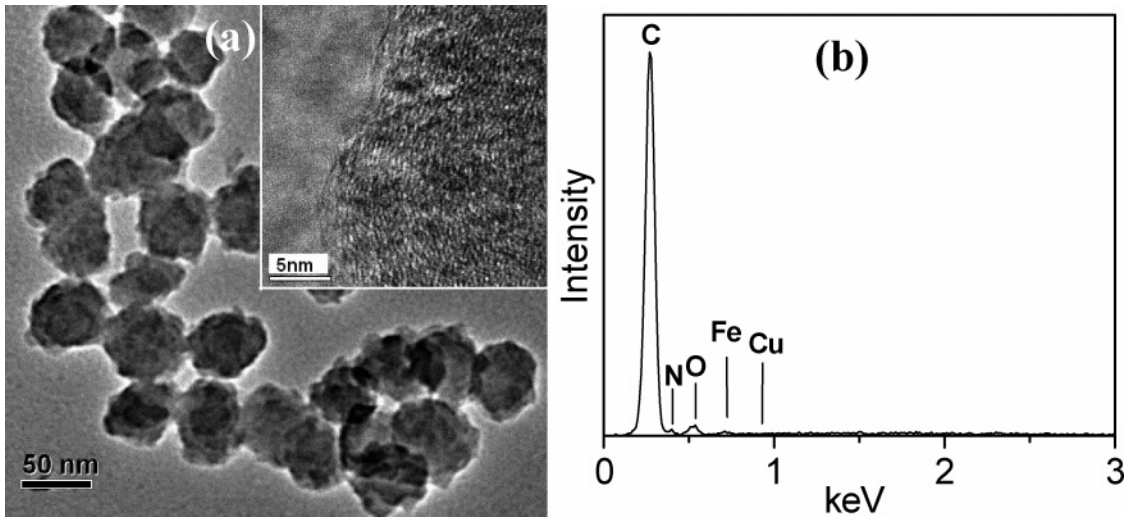

Figure 3. TEM image (a) and EDX spectrum (b) of CNS-2.

are assigned to (002) and (101) planes of carbon materials, respectively, suggesting a turbostratic structure of CNS-2 with a large curvature of the graphene layers.[35] In contrast to the previously reported results,[15] the signals due to Fe species cannot be observed. The XRD pattern of sample PNS-2 also exhibits a weak and broad peak at 25.2° 2θ, indicating an amorphous structure of Ppy, consistent with the literature results.[36] Figure 4b shows the first-order Raman spectrum of sample CNS-2. The first-order spectrum of CNS-2 exhibits two broad and strongly overlapping peaks. The peak at ~1345 cm^{-1} (disorder-induced D band) is attributed to A_{1g} model and is associated with the presence of structural defects and disorders of carbon materials, while the peak at ~1580 cm^{-1} (G band) has E_{2g} symmetry and is related to the vibration of sp^2-bonded carbon atoms in a two-dimensional hexagonal lattice, resulting from the stretching modes of C═C bonds of typical graphite. The relative intensity ratio of the D- and G-bands, $I_D/I_G = 0.95$, indicates that the CNS-2 belongs to a turbostratic structure

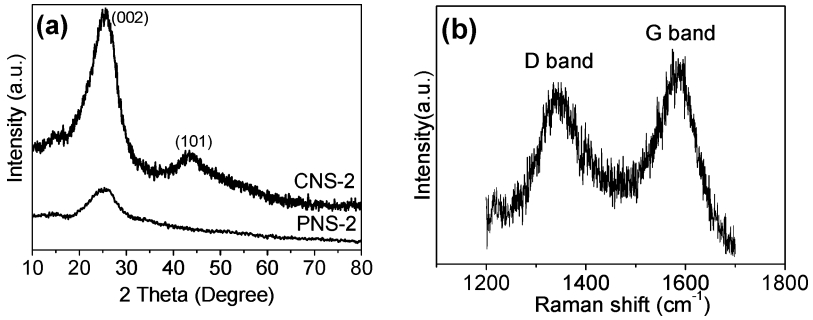

Figure 4. (a) XRD patterns of PNS-2 and CNS-2 and (b) Raman spectrum of CNS-2.

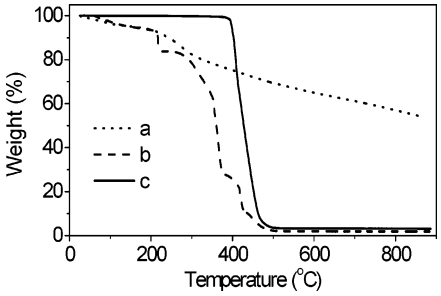

Figure 5. TG curves: (a) PNS-2 in nitrogen; (b) PNS-2 in air; and (c) CNS-2 in air.

composed of roughly parallel short graphene sheets, consistent with the TEM observation in Figure 3a and XRD result in Figure 4a.

3.4. Thermogravimetric Analysis. The TGA curves of samples PNS-2 and CNS-2 are shown in Figure 5. The TG curve of PNS-2 in nitrogen demonstrates that the weight lost was stepwise in the whole temperature range (Figure 5a), which indicates a complex thermal process. The residual weight at 870 °C was estimated to be ∼54 wt %, which is consistent with the carbonization yield of CNS-2 at 900 °C in our preparation experiment (∼50−55 wt %). Comparing the TG curve of sample PNS-2 (see Figure 5b) with that of CNS-2 (see Figure 5c) in air before 400 °C, the weight loss for CNSs was much lower (∼2 wt %) while the weight loss for PNSs was considerable (∼75 wt %), demonstrating the transformation of a thermally unstable polymer to a stable carbon material during the carbonization process. The residual weights for PNSs and CNSs above 600 °C in air were around 2.0 wt % and 3.7 wt %, respectively, which are attributed to the presence of Fe species in both products. Importantly, it can be clearly observed that the rapid decrease in weight for CNSs in air began at ∼400 °C and ended at 500 °C. This can be attributed to the presence of Fe species and a large number of graphene layer defects such as dangling bonds, edges, and vacancies, which enable oxygen to readily permeate the spheres, facilitating rapid oxidation.[37]

3.5. XPS Analysis. The XPS survey spectra of samples PNS-2 and CNS-2 are depicted in Figure 6. The presence of C and O elements is clearly seen in wide spectra for both samples. The N_{1s} spectrum of sample PNS-2 in the inset of Figure 6a shows one peak with a binding energy (BE) of 399.1 eV, corresponding to N atoms within the pentagonal pyrrole ring of the Ppy, in good agreement with a previous report.[38] Two peaks of the N_{1s} spectrum for sample CNS-2 in the inset of Figure 6b can be seen. These peaks are associated with pyridine-type N atoms existing at the edge of the graphene sheets (the peak with a BE of 397.8 eV) and quaternary N atoms incorporated in the graphene sheets (the peak with a BE of 400.7 eV).[28] The data indicates that N atoms within the pentagonal ring of the Ppy chemical structure were converted to two types of N atoms incorporated with carbon atoms within graphene aromatic structure after carbonization. The mass weight of the C, N, and O elements for CNS-2 calculated from the corresponding peak areas are 88.9, 5.5, and 5.6 wt %, respectively, approximately consistent with the results of EDX analysis in Figure 4b. The iron signal was not detected in CNS-2 and PNS-2, presumably due to the Fe species incorporated within the interior of carbon or polymer particles or lower levels on the particle surface. The BET surface areas for CNS-1, CNS-2, and CNS-3 are around 49, 55, and 59 m^2/g, respectively.

3.6. Electrochemical Properties of CNSs as Anode Materials for Lithium-Ion Batteries. Sample CNS-2 was evaluated as a representative sample in terms of its electrochemical performance in lithium-ion batteries. The first cycle charge and discharge curve shown in Figure 7 represents the curve trend of non-graphite carbon. In the first cycle, a specific capacity of 423 mAh/g was observed and Coulombic efficiency was calculated to be ∼72.6%. As seen from the cycling curves of Figure 8a, this sample demonstrates a reversible capacity of ∼420 mAh/g at a current of 60 mA/g, which is higher than the theoretical value of graphite (∼372 mAh/g) and that of graphitizable hollow carbon spheres (330 mAh/g) at the same current[28] but is comparable to that of hard carbon spheres derived from sucrose.[39] It can also be seen that the cyclability of CNSs at 60 mA/g (∼0.15% capacity loss per cycle after 60 cycles) is obviously better than that of hard carbon spheres enhanced by B_2O_3 at 23 mA/g (∼1.12% loss per cycle after 19 cycles).[40] In principle, the cyclability of CNSs at 23 mA/g should be better than that at a current of 60 mA/g. This improvement is possibly due to the smaller particle size of CNSs since the particle size of carbon spheres prepared from sucrose is generally larger.[41]

The rate capability of sample CNS-2 was also evaluated and is shown in Figure 8b. The measured rate capability of CNS-2 was much better than that of commercial mesophase carbon microbeads (MCMBs)[42] and even better than that of graphitized carbon nanobeads (average particle size of 200 nm).[20] This can be attributed to the improvement of lithium ion diffusion in the CNS electrode,[26,27,29] which has a particle size of <100 nm in diameter. The other reasons such as nitrogen-doping[28] and the low resistance of the solid electrolyte interface (SEI) film derived from the unique nanostructure of CNSs with a reasonable surface area[20] may contribute to this enhancement. Since the surface of CNSs is built with graphene layers as shown in the inset of Figure 3a, lithium ions can intercalate into the CNSs at the defect sites of the edge plane, which is responsible for the formation of the SEI.[20,43] Therefore, a moderate decomposition of electrolytes may occur on the surface of the CNSs to bring about a small SEI resistance because of the small surface area. For porous carbon materials, their extremely high surface area normally creates excessive side reactions with the electrolyte, forming SEI to inhibit reversible faradaic reaction. This

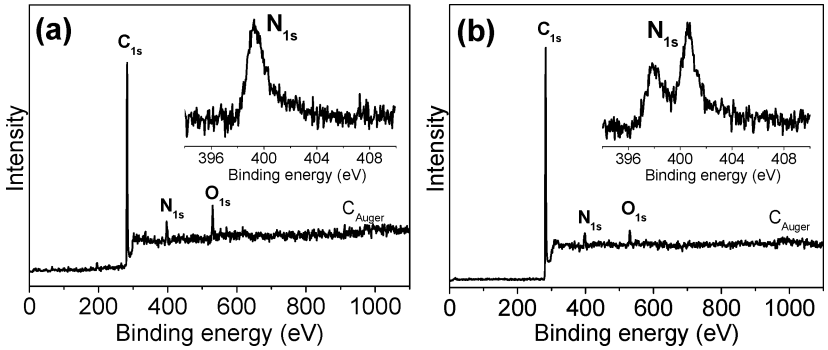

Figure 6. XPS wide and N_{1s} (inset) spectra of PNS-2 (a) and CNS-2 (b).

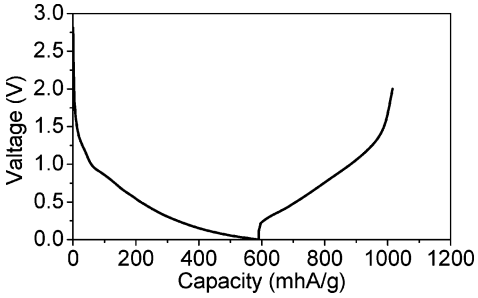

Figure 7. First cycle charge and discharge curve of sample CNS-2.

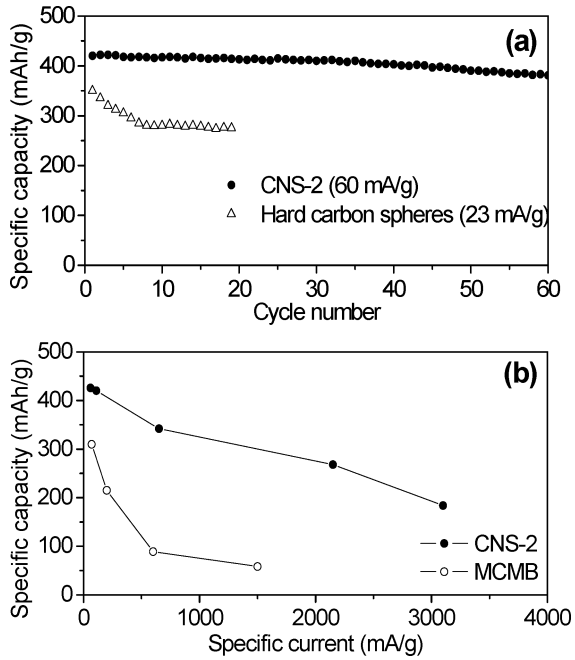

Figure 8. Electrochemical properties of sample CNS-2: (a) cycling performance (the cycling values of hard carbon spheres were cited from ref 40) and (b) rate performance (2 V−5 mV).

gives rise to a larger irreversible capacity loss in the first cycle and poor cyclic stability, which are undesirable in practical applications. It has been reported that the effect of a small amount of iron species in CNSs (3.9 wt %) on electrochemical properties could be neglected.[44]

4. Conclusions

In summary, monodisperse polypyrrole nanospheres (PNSs) with a controllable particle size have been synthesized using ultrasonic polymerization of pyrrole monomer in the presence of dual surfactants with ferric chloride ($FeCl_3$) as an oxidizing catalyst. Dense carbon nanospheres (CNSs) with diameters ranging from 50 to 100 nm have been obtained by carbonizing PNSs under nitrogen atmosphere. The CNSs were observed to display a higher specific capacity than hard carbon spheres derived from sucrose and a higher rate capability than commercial mesophase carbon microbeads in lithium-ion batteries.

Acknowledgment

The authors gratefully acknowledge NUS, the Engineering, Physical Sciences Research Council of U.K. (EPSRC, EP/C511794/1), National Natural Science Foundation of China (50701029), and Shanghai Pujiang Program (07pj14042) for financial support.

Literature Cited

(1) Serp, P.; Feurer, R.; Kalck, P.; Kihn, Y.; Faria, J. L.; Figueiredo, J. L. A Chemical Vapour Deposition Process for the Production of Carbon Nanospheres. *Carbon* **2001**, *39*, 621.

(2) Jin, Y. Z.; Gao, C.; Hsu, W. K.; Zhu, Y.; Huczko, A.; Bystrzejewski, M.; Roe, M.; Lee, C. Y.; Acquah, S.; Kroto, H.; Walton, D. R. M. Large-Scale Synthesis and Characterization of Carbon Spheres Prepared by Direct Pyrolysis of Hydrocarbons. *Carbon* **2005**, *43*, 1944.

(3) Pol, V. G.; Motiei, M.; Gedanken, A.; Calderon-Moreno, J.; Yoshimura, M. Carbon Spherules: Synthesis, Properties and Mechanistic Elucidation. *Carbon* **2004**, *42*, 111.

(4) Ma, X.; Xu, F.; Chen, L.; Zhang, Y.; Zhang, Z.; Qian, J.; Qian, Y. Easy Nickel Substrate-Assisted Growth of Uniform Carbon Microspheres and Their Spectroscopic Properties. *Carbon* **2006**, *44*, 2861.

(5) Tosheva, L.; Parmentier, J.; Valtchev, V.; Vix-Guterl, C.; Patarin, J. Carbon Spheres Prepared from Zeolite Beta Beads. *Carbon* **2005**, *43*, 2474.

(6) Zhou, Z.; Yan, Q.; Su, F.; Zhao, X. S. Replicating Novel Carbon Nanostructures with 3D Macroporous Silica Template. *J. Mater. Chem.* **2005**, *15*, 2569.

(7) Wang, Q.; Li, H.; Chen, L.; Huang, X. Monodispersed Hard Carbon Spherules with Uniform Nanopores. *Carbon* **2001**, *39*, 2211.

(8) Sun, X.; Li, Y. Colloidal Carbon Spheres and Their Core/Shell Structures with Noble-Metal Nanoparticles. *Angew. Chem., Int. Ed.* **2004**, *43*, 597.

(9) Yao, J.; Wang, H.; Liu, J.; Chan, K.-Y.; Zhang, L.; Xu, N. Preparation of Colloidal Microporous Carbon Spheres from Furfuryl Alcohol. *Carbon* **2005**, *43*, 1709.

(10) Zhang, X.; Manohar, S. K. Microwave Synthesis of Nanocarbons from Conducting Polymers. *Chem. Commun.* **2006**, 2477.

(11) Jang, J.; Oh, J. H. Novel Crystalline Supramolecular Assemblies of Amorphous Polypyrrole Nanoparticles through Surfactant Templating. *Chem. Commun.* **2002**, 2200.

(12) Jang, J.; Li, X. L.; Oh, J. H. Facile Fabrication of Polymer and Carbon Nanocapsules Using Polypyrrole Core/Shell Nanomaterials. *Chem. Commun.* **2004**, 794.

(13) Ding, L.; Olesik, S. V. Carbon Microbeads Produced through Synthesis and Pyrolysis of Poly(1,8-Dibutyl-1,3,5,7-Octatetrayne). *Chem. Mater.* **2005**, *17*, 2353.

(14) Kim, B. J.; Chang, J. Y. Preparation of Carbon Nanospheres from Diblock Copolymer Micelles with Cores Containing Curable Acetylenic Groups. *Macromolecules* **2006**, *39*, 90.

(15) Jang, J.; Yoon, H. Multigram-Scale Fabrication of Monodisperse Conducting Polymer and Magnetic Carbon Nanoparticles. *Small* **2005**, *1*, 1195.

(16) Henry, M. C.; Hsueh, C.-C.; Timko, B. P.; Freunda, M. S. Reaction of Pyrrole and Chlorauric Acid A New Route to Composite Colloids. *J. Electrochem. Soc.* **2001**, *148*, D155.

(17) Zhang, X.; Manohar, S. K. Bulk Synthesis of Polypyrrole Nanofibers by a Seeding Approach. *J. Am. Chem. Soc.* **2004**, *126*, 12714.

(18) Jang, J.; Yoon, H. Fabrication of Magnetic Carbon Nanotubes Using a Metal-Impregnated Polymer Precursor. *Adv. Mater.* **2003**, *15*, 2088.

(19) Zhang, X.; Manohar, SK. Narrow Pore-Diameter Polypyrrole Nanotubes. *J. Am. Chem. Soc.* **2005**, *127*, 14156.

(20) Wang, H.; Abe, T.; Maruyama, S.; Iriyama, Y.; Ogumi, Z.; Yoshikawa, K. Graphitized Carbon Nanobeads with an Onion Texture as a Lithium-Ion Battery Negative Electrode for High-Rate Use. *Adv. Mater.* **2005**, *17*, 2857.

(21) Yoshizawa, N.; Tanaike, O.; Hatori, H.; Yoshikawa, K.; Kondo, A.; Abe, T. TEM and Electron Tomography Studies of Carbon Nanospheres for Lithium Secondary Batteries. *Carbon* **2006**, *44*, 2558.

(22) Yoon, H.; Ko, S.; Jang, J. Nitrogen-Doped Magnetic Carbon Nanoparticles as Catalyst Supports for Efficient Recovery and Recycling. *Chem. Commun.* **2007**,1468.

(23) Yan, A.; Lau, B. W.; Weissman, B. S.; Külaots, I.; Yang, N. Y. C.; Kane, A. B.; Hurt, R. H. Biocompatible, Hydrophilic, Supramolecular Carbon Nanoparticles for Cell Delivery. *Adv. Mater.* **2006**, *18*, 2373.

(24) Sun, Y. P.; Zhou, B.; Lin, Y.; Wang, W.; Fernando, K. A. S.; Pathak. P.; Meziani, M. J.; Harruff, B. A.; Wang, X.; Wang, H.; Luo, P. G.; Yang, H.; Kose, M. E.; Chen, B.; Veca, L. M.; Xie, S.-Y. Quantum-Sized Carbon Dots for Bright and Colorful Photoluminescence. *J. Am. Chem. Soc.* **2006**, *128*, 7756.

(25) Cao, L.; Wang, X.; Meziani, M. J.; Lu, F.; Wang, H.; Luo, P. G.; Lin, Y.; Harruff, B. A.; Veca, L. M.; Murray, D.; Xie, S.-Y.; Sun, Y.-P. Carbon Dots for Multiphoton Bioimaging. *J. Am. Chem. Soc.* **2007**, *129*, 11318.

(26) Su, F.; Zhao, X. S.; Wang, Y.; Zeng, J.; Zhou, Z.; Lee, J. Y. Synthesis of Graphitic Ordered Macroporous Carbon with a Three-Dimensional Interconnected Pore Structure for Electrochemical Applications. *J. Phys. Chem. B* **2005**, *109*, 20200.

(27) Lee, K. T.; Lytle, J. C.; Ergang, N. S.; Oh, S. M.; Stein, A. Synthesis and Rate Performance of Monolithic Macroporous Carbon Electrodes for Lithium-Ion Secondary Batteries. *Adv. Funct. Mater.* **2005**, *15*, 547.

(28) Su, F.; Zhao, X. S.; Wang, Y.; Wang, L.; Lee, J. Y. Hollow Carbon Spheres with a Controllable Shell Structure. *J. Mater. Chem.* **2006**, *16*, 4413.

(29) Wang, Z.; Li, F.; Ergang, N. S.; Stein, A. Effects Of Hierarchical Architecture on Electronic and Mechanical Properties of Nanocast Monolithic Porous Carbons and Carbon-Carbon Nanocomposites. *Chem. Mater.* **2006**, *18*, 5543.

(30) Ergang, N. S.; Lytle, J. C.; Lee, K. T.; Oh, S. M.; Smyrl, W. H.; Stein, A. Photonic Crystal Structures as a Basis for a Three-Dimensionally Interpenetrating Electrochemical-Cell System. *Adv. Mater.* **2006**, *18*, 1750.

(31) Wang, Y.; Lee, J. Y.; Chen, B. H. Microemulsion Syntheses of Sn and SnO_2-Graphite Nanocomposite Anodes for Li-Ion Batteries. *J. Electrochem. Soc.* **2004**, *151*, A563.

(32) Ashokkumar, M.; Hodnett, M.; Zeqiri, B.; Grieser, F.; Price, G. J. Acoustic Emission Spectra from 515 Khz Cavitation in Aqueous Solutions Containing Surface-Active Solutes. *J. Am. Chem. Soc.* **2007**, *129*, 2250.

(33) Suslick, K. S. Sonoluminescence and Sonochemistry. In *Encyclopedia of Physical Science and Technology*; Meyers, R. A., Ed.; Academic Press, Inc.: San Diego, CA, 2001; Vol. 17, p 363.

(34) Jang, J.; Oh, J. H.; Stucky, G. D. Fabrication of Ultrafine Conducting Polymer and Graphite Nanoparticles. *Angew. Chem., Int. Ed.* **2002**, *41*, 4016.

(35) Li, Z. Q.; Lu, C. J.; Xia, Z. P.; Zhou, Y.; Luo, Z. X-Ray Diffraction Patterns of Graphite and Turbostratic Carbon. *Carbon* **2007**, *45*, 1686.

(36) Chen, Y.-S.; Li, Y.; Wang, H.-C.; Yang, M.-J. Gas Sensitivity of a Composite of Multi-Walled Carbon Nanotubes and Polypyrrole Prepared by Vapor Phase Polymerization. *Carbon* **2007**, *45*, 357.

(37) Jin, Y. Z.; Kim, Y. J.; Gao, C.; Zhu, Y. Q.; Huczko, A.; Endo, M.; Kroto, H. W. High Temperature Annealing Effects on Carbon Spheres and Their Applications as Anode Materials in Li-Ion Secondary Battery. *Carbon* **2006**, *44*, 724.

(38) Zhang, X.; Bai, R. B. Surface Electric Properties of Polypyrrole in Aqueous Solutions. *Langmuir* **2003**, *19*, 10703.

(39) Wang, Q.; Li, H.; Chen, L.; Huang, X. Novel Spherical Microporous Carbon as Anode Material for Li-Ion Batteries. *Solid State Ionics* **2002**, *152*−*153*, 43.

(40) Wu, X.; Wang, Z.; Chen, L.; Huang, X. Carbon/B_2O_3 Composite with Higher Capacity for Lithium Storage. *Solid State Ionics* **2004**, *170*, 117.

(41) Alcántara, R.; Ortiz, G. F.; Lavela, P.; Tirado, J. L. EPR, NMR, and Electrochemical Studies of Surface-Modified Carbon Microbeads. *Chem. Mater.* **2006**, *18*, 2293.

(42) Alcántara, R.; Fernández Madrigal, F. J.; Lavela, P.; Tirado, J. L.; Jiménez Mateos, J. M.; Gómez de Salazar, C.; Stoyanova, R.; Zhecheva, E. Characterisation of Mesocarbon Microbeads (MCMB) as Active Electrode Material in Lithium and Sodium Cells. *Carbon* **2000**, *38*, 1031.

(43) Chung, G. C. Reconsideration of SEI stability: Reversible Lithium Intercalation into Graphite Electrodes in *Trans*-2,3-Butylene Carbonate. *J. Power Sources* **2002**, *104*, 7.

(44) Concheso, A.; Santamaría, R.; Menéndez, R.; Jiménez-Mateos, J. M.; Alcántara, R.; Lavela, P.; Tirado, J. L. Iron−Carbon Composites as Electrode Materials in Lithium Batteries. *Carbon* **2006**, *44*, 1762.

Received for review October 3, 2007
Revised manuscript received January 24, 2008
Accepted January 26, 2008

IE071337D